Primljen / Received: 10.7.2024.
Ispravljen / Corrected: 10.6.2025.
Prihvaćen / Accepted: 25.6.2025
Dostupno online / Available online: 10.9.2025.

Vertical-bending properties of composite box girder with corrugated steel web and steel bottom slab

Authors:

Prof. **Feng Cen**, PhD. CE
Nanjing University of Aeronautics and Astronautics, China
Department of Civil Engineering
glwzlwz@163.com
Corresponding author

Pei-wei Gao, MSc. CE
Nanjing University of Aeronautics and Astronautics, China
Department of Civil Engineering
18862326148@nuaa.edu.cn

Original research paper

Feng Cen, Pei-wei Gao

Vertical-bending properties of composite box girder with corrugated steel web and steel bottom slab

A composite box girder with corrugated steel webs and a steel bottom slab is a new type of steel–concrete structure that works primarily in the vertical-bending state. This study proposes a method to derive the governing differential equations and natural boundary conditions that define the additional deflection induced by the shear-lag effect as the generalised displacement. Two shear-lag longitudinal warping displacement difference functions were set for the cantilever and flange slabs of the box girder to accurately analyse its mechanical properties. The proposed equations are verified by experimental and numerical data. This equations reflect the vertical-bending mechanical properties of the composite box girder, including the non-uniform distribution of normal stress in the flange slabs and the influence of the accordion effect, shear lag, and self-equilibrium conditions.

Key words:
composite box girder, stress distribution, accordion effect, shear lag effect, self-equilibrium condition

Izvorni znanstveni rad

Feng Cen, Pei-wei Gao

Svojstva vertikalnog savijanja spregnutoga sandučastog nosača s čeličnim valovitim hrptom i čeličnom donjom pločom

Spregnuti sandučasti nosač s hrptom od valovitog čelika i čeličnom donjom pločom nova je vrsta čelično-betonske konstrukcije koja ponajprije preuzima opterećenja u stanju vertikalnog savijanja. U ovom se radu predlaže metoda za izvođenje diferencijalnih jednadžbi i pripadajućih rubnih uvjeta koji opisuju dodatne progibe izazvane učinkom zaostajanja posmika kao generalizirane pomake. Dvije funkcije razlike uzdužnih deformacija uslijed zaostajanja posmika postavljene su za konzolni dio i prirubnične ploče sandučastog nosača kako bi se omogućila precizna analiza njegovih mehaničkih svojstava. Predložene jednadžbe na kraju su potvrđene eksperimentalnim i numeričkim rezultatima. One vjerno odražavaju mehanička svojstva vertikalnog savijanja spregnutoga sandučastog nosača, uključujući neujednačenu raspodjelu normalnih naprezanja u prirubničkim pločama te utjecaje efekta harmonike, zaostajanja posmika i uvjeta samoravnoteže.

Ključne riječi:
spregnuti sandučasti nosač, raspodjela naprezanja, efekt harmonike, utjecaj zaostajanja posmika, uvjet samoravnoteže

1. Introduction

Prestressed concrete (PC) box-girder bridges are currently the most common type of long-span bridges worldwide. However, problems in their structural working performance and material properties have gradually emerged. For example, many PC box-girder bridges suffer from beam cracking and excessive deflection after several years of service [1-3]. French bridge experts first suggested replacing traditional PC box-girder webs with corrugated steel webs to reduce the strong mutual restraint between the flange slabs and webs of PC box girders with an accordion effect [4-7]. To date, more than 500 composite girder bridges have been built worldwide, including more than 200 in Japan and over 100 in China. These box girders are traditional composite box-girder bridges [7-10], which continue to suffer from cracking and crushing damage to the reinforced concrete (RC) bottom slab. This type of PC composite box girder also has a relatively high dead weight and complex construction process. Therefore, in recent years, Chinese scholars have proposed the improvement of RC bottom slabs using flat steel slabs [11, 12]. This resulted in the substantial reduction in dead weight, rapid construction, and opportunities to build in areas with large temperature differences, collapsible loess, and soft soil [11-14]. To date, simply supported, continuous, straight, and curved box-girder bridges have been built in China (Fig. 1). These bridges adopt the new type of composite box girders, such as the Dunhuang to Dangjin Mountain Expressway in Gansu Province and the reconstruction project of the entrance and departure overpass at Zhongchuan Airport with a span of up to 108 m [12]. However, because the composite box girders with corrugated steel (CS) webs and steel bottom (SB) slabs have a higher neutral axis, the stress on the SB slab is much greater than that on the top slab, which can cause yielding or buckling failure of the SB slab [14-16]. Furthermore, these problems limit the application of CS and SB box-girder bridges to some extent. To address this problem, scholars in China conducted an in-depth investigation into the mechanical properties of CS and SB box girders [11, 12]. Liu and Ma studied the static and dynamic characteristics of CS and SB box girders; however, they did not include self-equilibrium conditions for the shear-lag warping stress and bending moment. Wang et al. analysed the vertical-bending behaviour of a CS and SB box-girder structure using the energy-variation method and obtained an analytical solution [8, 9, 11, 12]. However, their study did not comprehensively consider the accordion effect, shear deformation, and shear lag, particularly the self-equilibrium conditions for the shear-lag warping stress and bending moment. In addition, the analytical results for the constraint conditions of simply supported box girders can be applied in limited engineering situations [11, 14]. With the development of bridge engineering, refined mechanical analyses have gradually become a requirement for safe designs [17-19]. Therefore, based on the energy-variation principle, this study established mechanical equations that determine the vertical-bending behaviour of CS and SB box-girder bridges, along with the introduction of self-equilibrium conditions and the accordion effect. A refined mechanical model and analytical results can provide a reference for the design of such structures, particularly continuous-beam bridges [20, 21].

2. Governing differential equation and natural boundary conditions

2.1. Longitudinal warping displacement function of flange slabs

Figure 2 shows the cross-section of a CS and SB box girder in the symmetrical bending state. w(z) and q(z) are the vertical deflection and vertical rotation angles of the section, respectively, related to elementary beam theory. $\nu_1(z)$ and $\nu_2(z)$ are the vertical deflections caused by the shear-lag effect of the cantilever slab and the upper and lower flange slabs, respectively. Here, the cantilever slab and upper and lower flange slabs are regarded as two independent shear-lag mechanical systems that satisfy self-equilibrium conditions. The longitudinal displacements of the cantilever slab and the upper and lower flange slabs should be the sum of the longitudinal warping displacement of box-girder flanges caused by the elementary beam theory, shear-lag effect, and interaction between shear-lag mechanical systems.

Figure 1. The construction and service state of composite box-girder bridges in China: a) The expressway bridge of Dunhuang to Dangjin mountain; b) The simply supported bridge at Jingzhong Airport

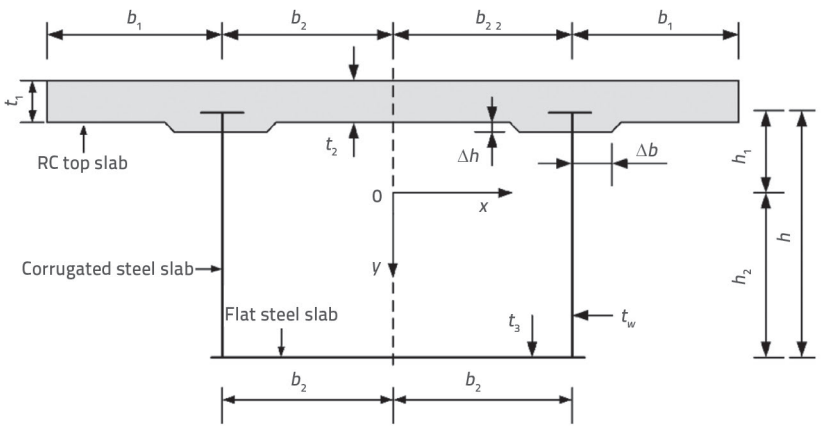

Figure 2. The cross-section of a CS and SB box girder

The longitudinal displacement of cantilever slabs (b_1) can be expressed as

$$u_1(x,y,z) = y\theta + [y - \alpha_1\omega_1(x) - \beta_1]v_1' + (y - \beta_2)v_2' \quad (1)$$

where $\omega_1(x) = 1 - (x^2 / b_1^2)$ is the non-uniform distribution function of the cantilever slab (b_1), α_1 and β_1 are correction factors for the cantilever slab (b_1) to satisfy the self-equilibrium conditions of the shear-lag warping stress and bending moment, respectively; and $b_2 \le x \le (b_1+b_2)$.

The shear-lag warping stress on the cantilever slabs (b_1) is

$$\sigma_{j1} = E[y - \alpha_1\omega_1(x)]v_1'' - E\beta_1 v_1' \quad (2)$$

where $\alpha_1 = \dfrac{3I}{4h_1b_1t_1}$ and $\beta_1 = \dfrac{-I}{h_1A}$ are the constant coefficients satisfying $\int_A \sigma_{j1}dA = 0$ and $\int_A \sigma_{j1}ydA = 0$, respectively.

The longitudinal displacement of the upper flange slabs (b_2) can be expressed as

$$u_2(x,y,z) = y\theta + [y - \alpha_2\omega_2(x) - \beta_2]v_2' + (y - \beta_1)v_1' \quad (3)$$

where $\omega_2(x) = 1 - (x^2/b_1^2)$ is the non-uniform distribution function, α_2 and β_2 are the correction factors for the upper and lower flange slabs to meet the self-equilibrium conditions of the shear-lag warping stress and bending moment, respectively; and $0 \le x \le b_2$.

The shear-lag warping stress on the top slab is

$$\sigma_{j2} = E[y - \alpha_2\omega_2(x)]v_2'' - E\beta_2 v_2'' \quad (4)$$

where the correction factors

$$\alpha_2 = \frac{3I}{2b_2(h_1t_2 - h_2\alpha_{Es}t_3)} \text{ and } \beta_2 = \frac{I(t_2 + \alpha_{Es}t_3)}{A(h_1t_2 - h_2\alpha_{Es}t_3)}$$

satisfy $\int_A \sigma_{j2}dA = 0 + \int_A \sigma_{j3}dA = 0$ and $\int_A \sigma_{j2}ydA = 0 + \int_A \sigma_{j2}ydA = 0$, A_1 and A_2 are the sectional areas of the cantilever and upper slabs, respectively; A_{sc} is the converted sectional area of the SB slab; and $A = A_1 + A_2 + A_{sc}$ is the total sectional area. In this study, the area of the SB slab was converted into the cross-sectional area of the hypothetical tensile concrete. Its sectional areas are $A_{sc} = \alpha_{Es}A_s$ and $\alpha_{Es} = E_s/E$, where E_s is the elastic modulus of the SB slab, E is the elastic modulus of the RC top slab, and A_s is the sectional area of the SB slab.

Meanwhile, $u_3(x, y, z)$ and σ_{j3} of the SB slab should be consistent with the form of the upper slab, but its y values are different.

2.2. Total potential energy of the CS and SB box girder

2.2.1. Total stress on slabs

The stress on the cantilever slab (b_1) is

$$\sigma_{z1} = Ey\theta' + E(y - \alpha_1\omega_1 - \beta_1)v_1'' + E(y - \beta_2)v_2'' \quad (5)$$

$$\tau_{j1} = G\frac{\partial u_1}{\partial x} \quad (6)$$

The stress on the upper flange slab (b_2) is

$$\sigma_{z2} = Ey\theta' + E(y - \alpha_2\omega_2 - \beta_2)v_2'' + E(y - \beta_1)v_1'' \quad (7)$$

$$\tau_{j2} = G\frac{\partial u_2}{\partial x} \quad (8)$$

The stress on the SB slab (b_2) is

$$\sigma_{z3} = Ey\theta' + E(y - \alpha_2\omega_2 - \beta_2)v_2'' + E(y - \beta_1)v_1' \quad (9)$$

$$\tau_{j3} = G\frac{\partial u_3}{\partial x} \quad (10)$$

2.2.2. Deformation potential energy of slabs

The deformation potential energy of the stress on the flange and cantilever slabs can be expressed as

$$U_1 = \frac{1}{2}\iiint \left(\frac{\sigma_{z1}^2}{E} + \frac{\tau_{j1}^2}{G} + \frac{\sigma_{z2}^2}{E} + \frac{\tau_{j2}^2}{G} + \frac{\sigma_{z3}^2}{E} + \frac{\tau_{j3}^2}{G}\right)dAdz \quad (11)$$

Through a sorting transformation, U_1 can be expressed as

$$U_1 = \frac{1}{2}\int_0^l EI(\theta')^2dz + \frac{1}{2}\int_0^l EI_1(v_1'')^2dz + \frac{1}{2}\int_0^l EI_2(v_2'')^2dz + \int_0^l EI_3(v_1''v_2'')dz + \\ + \int_0^l EI_4(\theta'v_1'')dz + \int_0^l EI_5(\theta'v_2'')dz + \frac{1}{2}\int_0^l GI_{G1}(v_1')^2dz + \frac{1}{2}\int_0^l GI_{G2}(v_2')^2dz \quad (12)$$

where

$$I = 2b_1t_1h_1^2 + 2b_2t_2h_1^2 + 2b_2\alpha_{Es}t_3h_2^2 + \frac{1}{6}b_1t_1^3 + \frac{1}{6}b_2t_2^3 + \frac{1}{6}b_2(\alpha_{Es}t_3)^3;$$

$$I_1 = I + \beta_1^2A + \frac{16}{15}\alpha_1^2b_1t_1 - \frac{8}{3}\alpha_1b_1t_1(\beta_1 - h_1);\quad I_{G1} = \frac{8\alpha_1^2t_1}{3b_1}$$

$$I_2 = I + \beta_2^2A + \frac{16}{15}\alpha_2^2b_2(t_2 + \alpha_{Es}t_3) + \frac{8}{3}\alpha_2b_2(h_2\alpha_{Es}t_3 - h_1t_2) + \frac{8}{3}\alpha_2\beta_2b_2(t_2 + \alpha_{Es}t_3)$$

$$I_{G2} = \frac{8\alpha_2^2}{3b_2}(t_2 + \alpha_{GS}t_3);\quad I_4 = 0;\quad I_5 = 0$$

$$I_3 = I + \beta_1\beta_2A + \frac{4}{3}\alpha_1b_1t_1(\beta_2 - h_1) + \frac{4}{3}\alpha_2b_2(h_2\alpha_{ES}t_3 - h_1t_2) + \frac{4}{3}\alpha_2\beta_1b_2(t_2 + \alpha_{ES}t_3)$$

I is the moment of inertia about the *x*-axis. When the shear strain energy is calculated, the area of the SB slab is converted into $A_{sG} = \alpha_{Gs}A_s$ and $\alpha_{Gs} = G_s/G$, where G_s and G are the shear moduli of the flat steel slab and RC top slab, respectively.
The Timoshenko shear strain energy is

$$U_j = \frac{1}{2}\int_0^l G_wA_w(w' - \theta)^2dz \tag{13}$$

where G_w and A_w are the modified shear modulus and effective shear area of the CS web, respectively.
The external loading-induced potential energy is

$$U_p = -\int_0^l q_y(z)[w(z) + v_1(z) + v_2(z)]dz - Q(z)[w(z) + v_1(z) + v_2(z)]\Big|_0^l + [M_1(z)v_1'(z) + M_2(z)v_2'(z) + M_z(z)\theta(z)]\Big|_0^l \tag{14}$$

where $M_1(z)$ and $M_2(z)$ are the bending moments about the *x*-axis caused by the shear-lag effect of the cantilever slab and the upper and lower flange slabs, respectively; $M_z(z)$ is the bending moment about the *x*-axis when the vertical rotation angle θ(z) is generated at the end of the beam segment; and Q(z) and $q_y(z)$ are the vertical shear forces at the end of the beam segment and the vertical distributed force on the box girder, respectively.
Then, the total potential energy of the CS and SB box girder is

$$U = U_1 + U_2 + U_p \tag{15}$$

2.3. Governing differential equations and natural boundary conditions

According to the energy-variation principle δU = 0, the governing differential equations and natural boundary conditions of the CS and SB box girder can be derived as

$$EI\theta'' + G_wA_w(w' - \theta) = 0 \tag{16}$$

$$G_wA_w(w'' - \theta') + q_y = 0 \tag{17}$$

$$[EI\theta' + M_z]\Big|_0^l\delta\theta = 0 \tag{18}$$

$$[G_wA_w(w' - \theta) + Q]\Big|_0^l\delta w = 0 \tag{19}$$

$$EI_1v_1^{(4)} + EI_3v_2^{(4)} - GI_{G1}v_1'' - q_y = 0 \tag{20}$$

$$EI_2v_2^{(4)} + EI_3v_1^{(4)} - GI_{G2}v_2'' - q_y = 0 \tag{21}$$

$$[EI_1v_1'' + EI_3v_2'' + M_1]\Big|_0^l\delta v_1' = 0 \tag{22}$$

$$[EI_1v_1^{(3)} + EI_3v_2^{(3)} - GI_{G1}v_1' - Q(z)]\Big|_0^l\delta v_1 = 0 \tag{23}$$

$$[EI_2v_2'' + EI_3v_1'' + M_2]\Big|_0^l\delta v_2' = 0 \tag{24}$$

$$[EI_2v_2^{(3)} + EI_3v_1^{(3)} - GI_{G2}v_2' - Q(z)]\Big|_0^l\delta v_2 = 0 \tag{25}$$

2.4. Solution of governing differential equations

By sorting and replacing Eq. (16) and (17), the solutions of equations w(z) and θ(z) can be obtained as

$$\theta(z) = c_1z^2 + c_2z + c_3 + \frac{q_y}{6EI}z^3 \tag{26}$$

$$w(z) = c_1\frac{z^3}{3} + \frac{-2EI}{G_wA_w}z + c_2\frac{z^2}{2} + c_3z + c_4 + \frac{-q_y}{2G_wA_w}z^2 + \frac{q_y}{24EI}z^4 \tag{27}$$

where c_1, c_2, c_3, c_4 are the constant coefficients of equations of w(z) and θ(z), which can be solved in accordance with the corresponding boundary conditions.
According to Eqs. (20) and (21), the following equation can be obtained.

$$v_1^{(6)} + \frac{G(I_{G1}I_2 + I_{G2}I_1)}{E(I_3^2 - I_2I_1)}v_1^{(4)} + \frac{-G^2I_{G2}I_{G1}}{E^2(I_3^2 - I_2I_1)}v_1'' + \frac{GI_{G2}}{E^2(I_3^2 - I_2I_1)}q_y = 0 \tag{28}$$

For Eq. (28), the solution of the eigenvalue equation can be given as $r_{1,2} = \pm h_1$; $r_{3,4} = \pm h_2$; $r_{5,6} = 0$. Then, the general solution of equation $v_1(z)$ can be expressed as

$$v_1(z) = e_1ch\eta_1z + e_2sh\eta_1z + e_3ch\eta_2z + e_4sh\eta_2z + e_5z + e_6 + \frac{-q_y}{2GI_{G1}}z^2 \tag{29}$$

According to Eq. (29) and the properties of an ordinary differential equation, the expression of the $v_2(z)$ solution was assumed. By substituting Eq. (29) into Eqs. (20) and (21), the constant coefficients of $v_2(z)$ can be obtained in accordance with the principle of identity; that is

$$v_2(z) = e_1B_1ch\eta_1z + e_2B_1sh\eta_1z + e_3B_3ch\eta_2z + e_4B_3sh\eta_2z + e_7z + e_8 + \frac{-q_y}{2GI_{G2}}z^2 \tag{30}$$

where

$$B_1 = \frac{\eta_1^2 + T_1}{T_2\eta_1^2};\ B_3 = \frac{\eta_2^2 + T_1}{T_2\eta_2^2};\ T_1 = \frac{-GI_{G1}}{EI_1};\ T_2 = \frac{-I_3}{I_1}$$

and e_1, ..., e_8 constant coefficients of equations of $v_1(z)$ and $v_2(z)$, which can be solved in accordance with the corresponding boundary conditions.

3. Common boundary conditions of CS and SB box girder

According to Eqs. (18), (19), (22), and (25), the specific boundary conditions of the CS and SB box girders can be obtained. For instance, the boundary conditions of the simply supported beam can be obtained, as shown in the following sections.

3.1. Uniform load

a) Boundary conditions relating w(z) and θ(z):

$$w(z)\big|_0^{l}=0;\ \theta(z)\big|_0^{l}=0 \tag{31}$$

b) Boundary conditions related $v_1(z)$ and $v_2(z)$:

$$v_1(z)\big|_0^{l}=0;\ v_2(z)\big|_0^{l}=0;v_1''(z)\big|_0^{l}=0;\ v_2''(z)\big|_0^{l}=0 \tag{32}$$

3.2. Concentrated load

As shown in Fig. 3, the boundary distances to the adjacent concentrated force P_k are L_{k1} and L_{k2}.

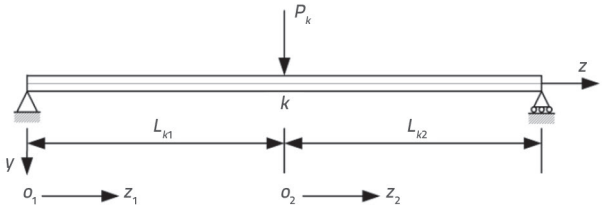

Figure 3. Coordinate system of simply supported CS and SB box girders under concentrated load opterećenjem

The numerical values in the subscripts of w(z) and $\theta(z)$ epresent the z_1 or z_2 coordinate systems, respectively. The boundary condition can then be obtained as

a) Boundary conditions relating w(z) and θ(z):

$$\begin{aligned}
&w_1(0)=0;\ w_2(L_{k2})=0;\ \theta_1(0)=0;\ \theta_2'(L_{k2})=0;\\
&w_1(L_{k1})=w_2(0);\ w_1'(L_{k1})=w_2'(0);\ \theta_1'(L_{k1})=\theta_2'(0)\\
&\theta_1(L_{k1})-\theta_2(0)=\frac{P_k}{G_wA_w}
\end{aligned} \tag{33}$$

b) Boundary conditions related $v_1(z)$ and $v_2(z)$:

The numerical values in the subscript parentheses of $v_1(z)$ and $v_2(z)$ represent its z_1^- or z_2^- coordinate system (as shown in Fig. 3). Then, the boundary condition can be obtained as

$$\begin{aligned}
&v_{1(1)}(0)=0;\ v_{1(2)}(L_{k2})=0;\ v_{1(1)}''(0)=0\\
&v_{1(2)}''(0)=0;\ v_{2(1)}(0)=0;\ v_{2(2)}(L_{k2})=0;\ v_{2(1)}''(0)=0;\\
&v_{2(2)}''(L_{k2})=0;\ v_{1(1)}(L_{k1})=v_{1(2)}(0);\ v_{1(1)}'(L_{k1})=v_{1(2)}'(0);\\
&v_{1(1)}''(L_{k1})=v_{1(2)}''(0);\ v_{2(1)}(L_{k1})=v_{2(2)}(0);\\
&v_{2(1)}'(L_{k1})=v_{2(2)}'(0);\ v_{2(1)}''(L_{k1})=v_{2(2)}''(0);\\
&[EI_1v_{1(1)}^{(3)}(L_{k1})+EI_3v_{2(1)}^{(3)}(L_{k1})]-[EI_1v_{1(2)}^{(3)}(0)+EI_5v_{2(2)}^{(3)}(0)]=-P_k;\\
&[EI_2v_{2(1)}^{(3)}(L_{k1})+EI_3v_{1(1)}^{(3)}(L_{k1})]-[EI_2v_{2(2)}^{(3)}(0)+EI_5v_{1(2)}^{(3)}(0)]=-P_k
\end{aligned} \tag{34}$$

Similarly, other specific boundary conditions can be obtained based on Eqs. (18) and (19) and (22) to (25).

4. Numerical analysis and experimental verification

An experimental model was constructed in accordance with the similarity principle to verify the mechanical properties of the CS and SB bridge. The CS webs and flat SB slabs were made of high-quality Q420 steel, with an elastic modulus of 206 GPa and a Poisson's ratio of 0.26. For the geometry of the corrugated web, L_1, L_2, L_3 are the length of the flat section, the length of the inclined slab section, and the projection of the inclined slab section on the horizontal plane of the CS web, respectively (as shown in Fig. 4). The CS web was t_w = 0.3 cm thick, and the beam was h = 0.4 m high. The top slab was made of C50 concrete with an average thickness of t_1 = t_2 = 5.2 cm, which was poured 13 months before the test. The flat SB slab thickness was t_3 = 0.5 cm, the lengths of the flange slabs were b_1 = 0.25 m and b_2 = 0.3 m, Δh = 2.5 cm and Δb = 3 cm. The total length of the model bridge was 6.2 m, and the calculated span was 6 m. The corrugated web and RC top slab were connected by embedded connecting keys. The embedded connecting keys were a flat steel bar 0.5 cm thick and 5 cm wide, welded to the top of the CS web every 15 cm longitudinally. The SB slab and CS web were also welded. The vertical concentrated load was P_k = 150 kN applied by the actuator. The uniform load was q_k = 26 kN/m and was applied using specially designed test blocks (as shown in Fig. 6). Figure 4 shows the layout of the strain gauges. One gauge was arranged every 5 cm at the top and bottom slabs at the mid-span and quarter-span sections. Twenty-three concrete strain gauges were arranged along the width of the top surface of the top slab (110 cm). Two strain gauges were arranged below the top slab (Fig. 4, 6^- and 18^-). Thirteen steel strain gauges were arranged below the SB slab (60 cm wide), and two strain gauges were arranged on the top surface of the SB slab (Fig. 4, 24^- and 36^-). The CS web was 34.8 cm high, and five longitudinal strain gauges were uniformly arranged along its height. A total of 50 concrete and 50 steel strain gauges were arranged to test the CS and SB box girders.

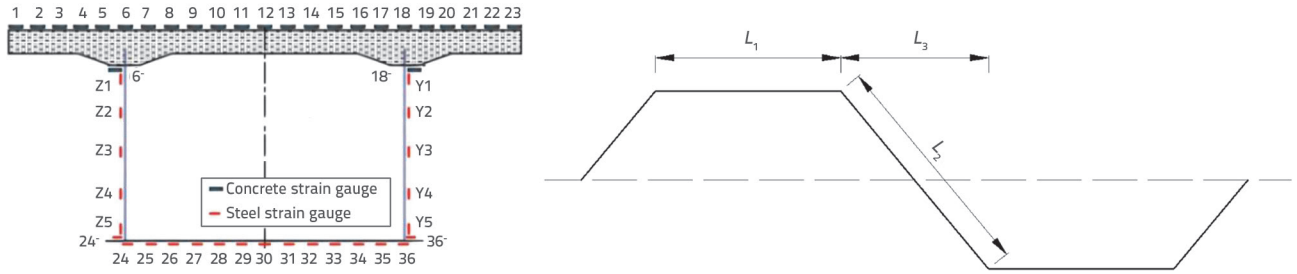

Figure 4. The strain gauge layout of the CS and SB box girder and the geometry of the corrugated web: a) The strain gauge layout for midspan and 1/4-span sections; b) Geometric shape of corrugated steel web

The constraint conditions of the simple and continuous beams are shown in Figs. 3 and 8. The experimental loading is shown in Figs. 6 and 8. The test data were the average values of four repeated loading tests up to a certain load level. A finite element model of the CS and SB box girders was established using the ANSYS finite element software, as shown in Fig. 5. The RC top and SB slabs adopted Solid65 elements, the diaphragm slabs adopted Solid45 elements, and the CS web adopted Shell63 elements. (The diaphragm slab was 10 cm thick, and five transverse diaphragm slabs were evenly set.) To connect the RC top slab and CS webs, the multipoint constraint method was applied [22]. The SB slab of the model bridge was connected to CS webs using a common joint mode.

The stress calculation section of the simply supported beam was at the mid-span, and the continuous beam was at bearing 0_2 between spans. This is the first time that these experimental results were published.

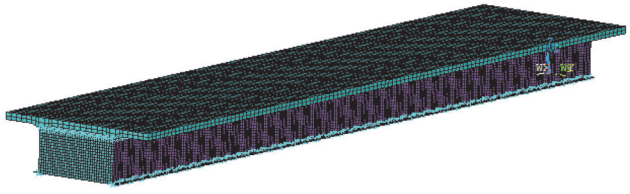

Figure 5. Finite element model of the CS and SB

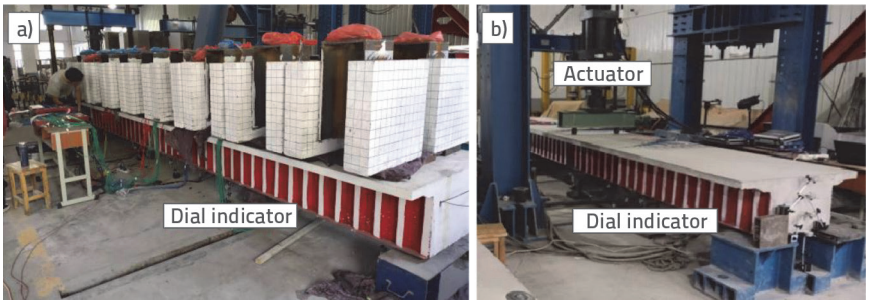

Figure 6. Experimental study of a simply supported CS and SB box girder: a) Uniform load; b) Concentrated load

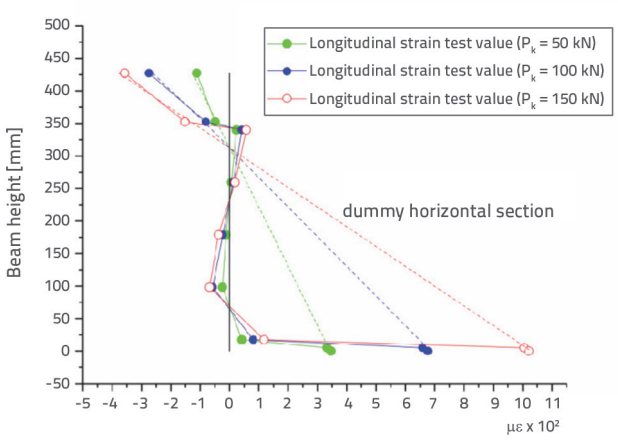

Figure 7. The experimental values of longitudinal strain distribution along beam height *h*

The strain values were the average strain values of the corresponding positions of the web slabs and top and bottom slabs on both sides at the mid-span section of the CS and SB box girder (as shown in Fig. 4). Figure 7 shows that the strain values at each measurement point within the height range of the CS web were extremely small — close to zero. Therefore, the cross-sectional deformation of the CS and SB box girders did not comply with the 'assumption of a flat cross-section'. However, if the strain distribution points within the height range of the CS web were removed, the longitudinal strain points of the upper and lower flange slabs could be connected to form a virtual plane, such that the longitudinal strain distribution of the upper and lower flange slabs could comply approximately with the 'dummy horizontal section assumption'. This was the theoretical foundation for analysing the vertical-bending mechanical performance of CS and SB box girders.

Table 1 lists the compressive stress values of the top slab of the simply supported CS and SB box girder for various calculation methods, as well as the shear-lag coefficients and accordion

Table 1. Stress distribution on the top slab of a simply supported composite box girder at the mid-span section (L_{k1} = L_{k2} = 3 m) (concentrated load)

Transverse coordinate of top slab centre as origin [m]	0	0.05	0.1	0.15	0.2	0.25	0.3	0.35	0.4	0.45	0.5	0.55
Theoretical value of elementary beam [MPa]	-8.74	-8.74	-8.74	-8.74	-8.74	-8.74	-8.74	-8.74	-8.74	-8.74	-8.74	-8.74
Influence value of shear-lag effect [MPa]	0.98	0.89	0.65	0.26	-0.25	-0.84	-1.47	-0.80	-0.19	0.30	0.61	0.72
Theoretical value of total stress in this study [MPa]	-7.76	-7.85	-8.09	-8.48	-8.99	-9.58	-10.21	-9.54	-8.93	-8.44	-8.13	-8.02
Finite element value [MPa]	-7.62	-7.68	-7.85	-8.12	-8.41	-9.04	-10.07	-8.95	-8.52	-8.12	-7.85	-7.74
Test value [MPa]	-7.72	-7.78	-7.96	-8.65	-8.82	-9.37	-10.34	-9.25	-9.13	-8.62	-8.02	-7.93
Shear-lag coefficient	0.89	0.90	0.93	0.97	1.03	1.10	1.17	1.09	1.02	0.97	0.93	0.92
Theoretical value of total stress (with flat steel web) [MPa]	-8.13	-8.22	-8.48	-8.88	-9.42	-10.04	-10.70	-9.99	-9.35	-8.84	-8.52	-8.40
Stress (with traditional theory) [MPa]	-7.84	-7.92	-8.13	-8.49	-9.00	-9.65	-10.45	-9.61	-8.95	-8.48	-8.20	-8.11
Influence ratio of two algorithms [%]	-1.02	-0.88	-0.49	-0.12	-0.11	-0.73	-2.30	-0.73	-0.22	-0.47	-0.85	-1.11
Accordion effect [%]	-4.55	-4.50	-4.60	-4.51	-4.57	-4.58	-4.58	-4.51	-4.49	-4.53	-4.58	-4.52

Note: The theoretical value in this study is the sum of the theoretical value of elementary beam and the influence value of shear lag. The elementary beam theory is a theory that does not consider shear lag effect, the traditional theory is a theory that does not consider the self -equilibrium conditions of shear warping stress, and the shear-lag coefficient is the ratio of the theoretical value in this paper and the theoretical value of the elementary beam. The same below.

Table 2. Stress distribution in the bottom slab of a simply supported composite box girder at the mid-span section (L_{k1} = L_{k2} = 3 m) (concentrated load)

Transverse coordinate with the centre of steel bottom slab as the origin [m]	0	0.05	0.1	0.15	0.2	0.25	0.3
Theoretical value of total stress on steel bottom slab [MPa]	157.95	159.65	164.63	172.55	182.87	194.89	207.79
Finite element value [MPa]	154.87	156.62	160.02	166.51	174.26	186.72	203.02
Test value [MPa]	159.24	160.47	162.32	178.68	186.75	196.13	211.34
Shear-lag coefficients	0.90	0.91	0.93	0.98	1.04	1.11	1.18
Stress on top slab with traditional theory [MPa]	154.32	155.74	160.01	167.13	177.10	189.91	205.57
Theoretical value of total stress on steel bottom slab (flat steel web) [MPa]	132.44	133.61	137.02	142.46	149.55	157.80	166.66
Influence ratio of two algorithms [%]	2.35	2.51	2.89	3.24	3.26	2.62	1.08
Accordion effect [%]	19.26	19.49	20.15	21.12	22.28	23.50	24.68

effect. It shows that the theoretical value in this study was the sum of the theoretical value of the elementary beam and the influence value of the shear-lag effect. Table 2 lists the tensile stress values of the bottom slab of the simply supported CS and SB box girder, showing that the stress values of the bottom slab at the corresponding positions were approximately 20 times that of the top slab. According to the above results, the mechanical properties of the CS and SB box girder comprise two independent systems: the elementary beam theory system and shear-lag mechanics system. No coupling relationship exists between them, which is the innovation of this study.

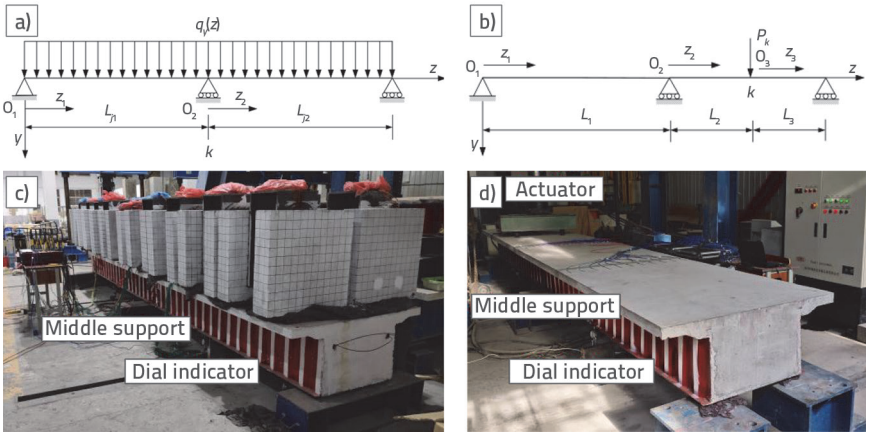

Figure 8. Experimental study of continuous CS and SB box girder under uniform and concentrated loads: Two-span girder under uniform load; b) Two-span girder under concentrated load; c) Continuous model beam test under uniform load; d) Continuous model beam test under concentrated load

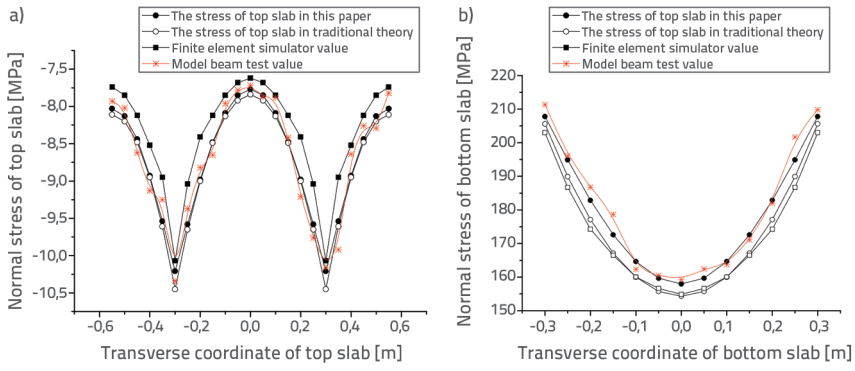

Figure 9. Stress comparison of simply supported CS and SB box girder at the mid-span section under concentrated load (L_{k1} = L_{k2} = 3 m): a) Stress distribution on the top slab; b) Stress distribution on the bottom slab

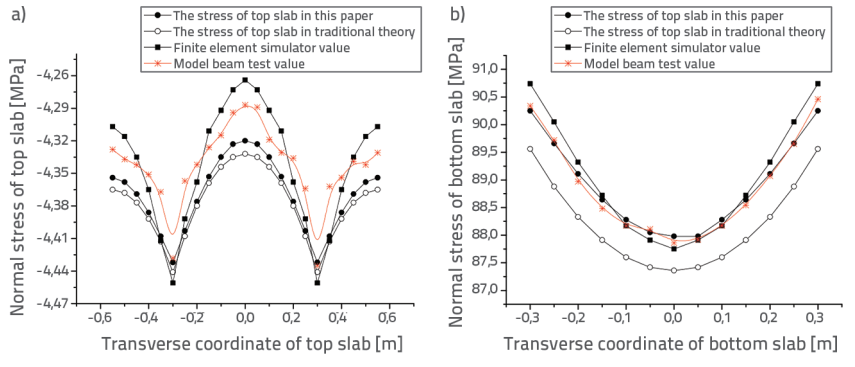

Figure 10. Stress comparison of simply supported CS and SB box girder under uniform load (L = 6 m): a) Stress distribution on the top slab; b) Stress distribution on the bottom slab

Figures 9–12 demonstrate that the following:

- For the simply supported and continuous CS and SB box girders, the normal stress distributions of the top and bottom slabs were uneven under the influence of the shear-lag effect, which significantly affected the mechanical properties of the girder. The theoretical values were in good agreement with those obtained from the finite element simulation and experiment, thereby demonstrating the validity of the proposed mechanical model. In particular, the CS and SB box girder had a higher neutral axis, resulting in lower stress on the top RC slab and excessive stress on the flat SB slab. For example, the normal stress on the SB slab of the model beam was greater than 20 times that on the RC top slab. Therefore, designers should carefully consider the mechanical properties of composite bridges.
- The traditional algorithm used the shear-lag theory without considering the self-equilibrium condition for the shear-lag warping stress and bending moment. Figures 9 and 10 show that for the simply supported CS and SB box girders, the influence of self-equilibrium conditions was minimal and could be ignored. However, the influence of self-equilibrium conditions on the continuous CS and SB box girders was substantial. Therefore, the mechanical analysis of continuous CS and SB box girders should consider the self-equilibrium conditions (see Figs. 11 and 12).

The shear-lag coefficient is the ratio of the theoretical value in this study and the theoretical value of the elementary beam. Figure 13 demonstrates the following:

- For a simply supported boundary condition, the shear-lag effect of the CS and SB box girders under a concentrated load exceeded that under a uniformly distributed load.

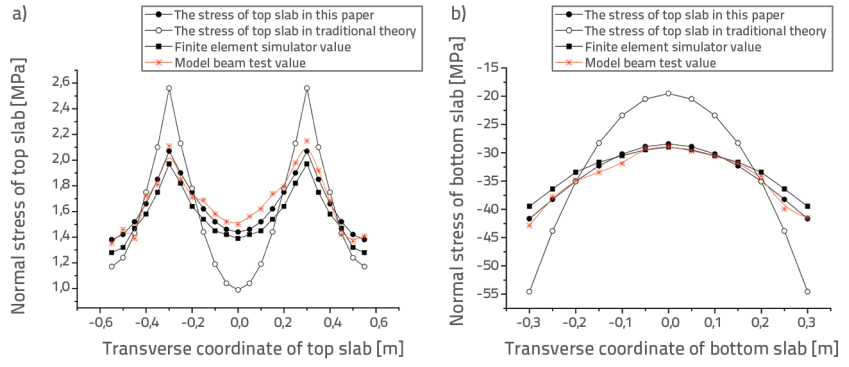

Figure 11. Stress comparison between continuous CS and SB box girders under concentrated load ($L_2 = L_3 = 1.5$ m). The girders were at bearing 0_2: a) Stress distribution on the top slab; b) Stress distribution on the bottom slab

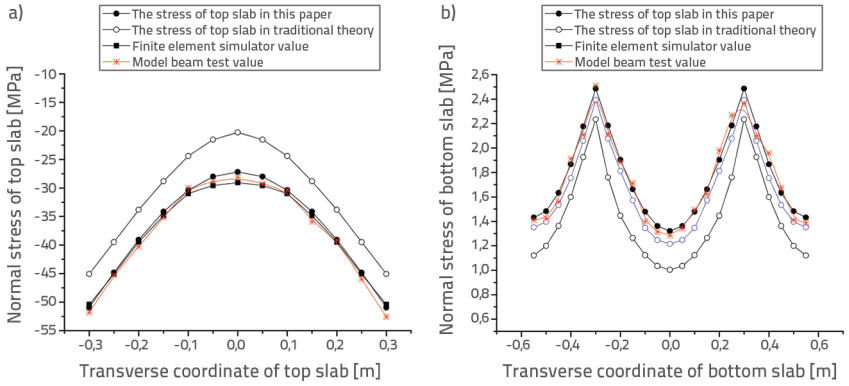

Figure 12. Stress comparison of continuous CS and SB box girders under uniform load ($L_{j1} = L_{j2} = 3$ m). The girders were at bearing 0_2: a) Stress distribution on the top slab; b) Stress distribution on the bottom slab

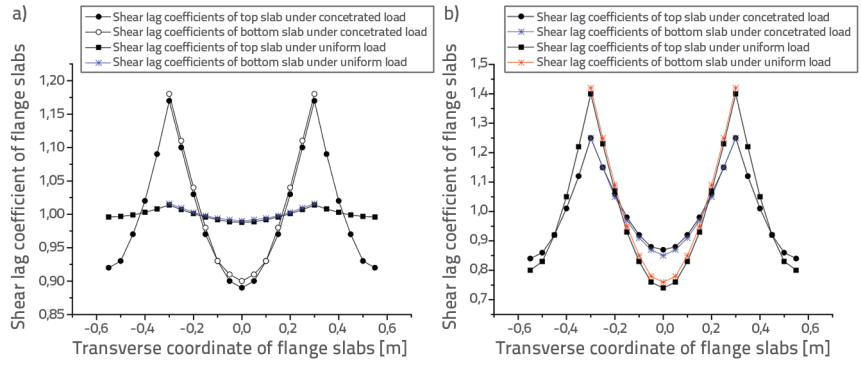

Figure 13. Shear-lag coefficients of top and bottom slabs of the CS and SB box girders: a) Shear-lag coefficients of the mid-span top and bottom slabs b) Shear-lag coefficients of the top and bottom slabs for a continuous for a simply supported box girder ($L_{k1} = L_{k2} = 3$ m, or $L = 6$ m) box girder ($L_1 = L_2 = 1.5$ m or $L_{j1} = L_{j2} = 3$ m) at bearing 0_2

For example, the shear-lag coefficient at the intersection of the top slab and web with a uniform load was 1.01, and that under a concentrated load was 1.17.

- The mechanical properties of the continuous CS and SB box girders underwent significant changes relative to the simply supported boundary conditions. For continuous CS and SB box girders, the influence of the shear-lag effect was more significant. For example, the shear-lag coefficient at the intersection of the top slab and web with a concentrated load was 1.25, and that under a uniform load was 1.40. This indicates that the stronger the constraint conditions, the more obvious the shear-lag effect. Compared with the simply supported CS and SB box girders, the shear-lag effect of the continuous CS and SB box girders was more prominent under a uniform load.

The accordion effect of the CS and SB box girders was defined as the stress ratio. This ratio is the stress difference between the corrugated and flat steel webs of the same thickness and the calculated stress value on a composite box girder with flat steel webs. Figure 14 shows the following:

- For simply supported box girders, the accordion effect of CS and SB box girders was closely related to the load distribution. When the load was uniformly distributed on the beam, the influence of the accordion effect was more uniform, and the accordion effect of CS and SB box girders under a concentrated load were greater. In particular, the accordion effect increased the tensile stress on the SB slab and reduced the compressive stress on the RC top slab. Compared with the top slab, the accordion effect had a greater effect on the mechanical properties of the SB slabs under a concentrated load. For example, the maximum influence ratio of the accordion effect at the intersection of

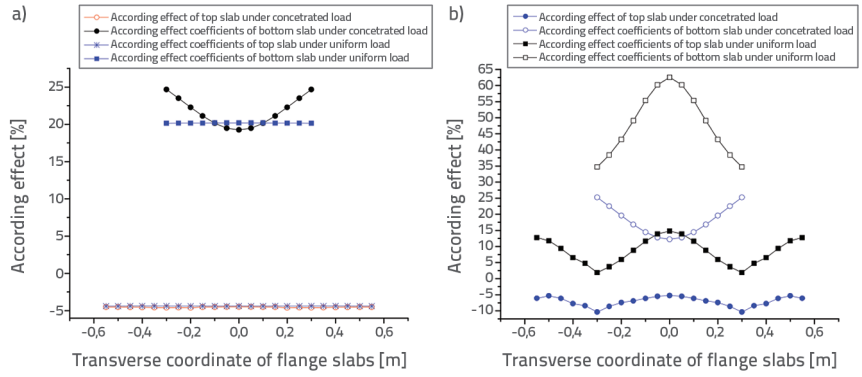

Figure 14. Comparison of the accordion effect for CS and SB box girders: a) At the mid-span section for a simply supported girder; b) At bearing 0_2 for a continuous girder

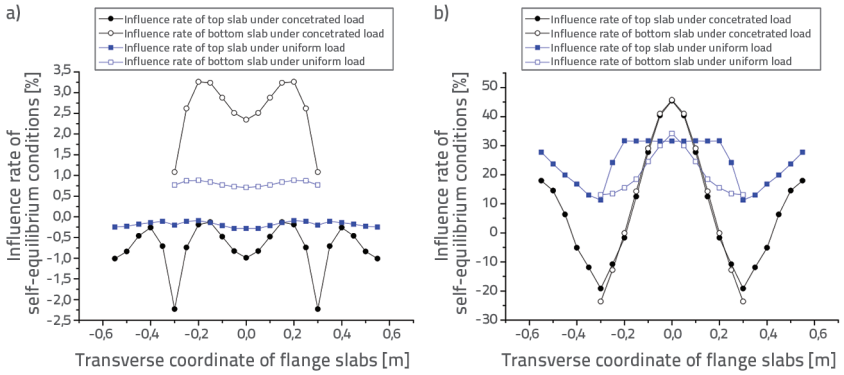

Figure 15. Influence rate of self-equilibrium conditions for the CS and SB box girder: a) Influence rate of self-equilibrium conditions on stress on flanges (b) Influence rate of self-equilibrium conditions on stress on flanges at the mid-span section for a simply supported box girder at bearing 0_2 for a continuous box girder

stress on the bottom slab of the continuous CS and SB box girder, which might cause buckling failure of the steel slab. The tensile stress on the RC top slab also increased under a uniform load, which can lead to cracking of the RC top slabs.

The traditional algorithm refers to the shear-lag theory without considering the self-equilibrium condition for shear-lag warping stress and bending moment. The influence rates of the self-equilibrium condition are the differences between the calculated stress values of this theory and the traditional theory, and its ratio to the calculated stress value of the traditional theory. Figure 15 shows the following:

- For simply supported CS and SB box girders, the maximum influence ratio of the self-equilibrium condition in this study is 3.3 %, and its minimum influence ratio is -2.2 %. Therefore, owing to the minor influence of self-equilibrium conditions on the stress on the top and bottom slabs, the influence of self-equilibrium conditions can be negligible for simply supported CS and SB box girders.

the SB slab and the web is 24.7 %. This implies that the tensile stress on the bottom slab of the CS and SB box girders was 24.7 % higher than that on the composite box girder with a flat steel web with the same thickness as that of corrugated steel webs. However, the accordion effect of the top slab is -4.6 %. This was beneficial because the compressive stress on the top slab was reduced.

- The accordion effect of the continuous CS and SB box girders significantly increased relative to the simply supported boundary condition. The main object of influence was still the SB slab. For example, the accordion effect at the intersection of the bottom slab and the web under a uniform load was 34.7 %, and that under a concentrated load was 25.2 %. Therefore, the accordion effect of a continuous CS and SB box girder was more prominent under uniform loads. Moreover, the accordion effect was greater at the transverse centre of the flange slabs, but the stress at that point was smaller; therefore, its actual effect was not prominent. Based on this, our research shows that the stronger the constraint conditions, the more pronounced the accordion effect. In particular, the accordion effect increased the compressive
- However, the influence of the self-equilibrium condition on the mechanical properties of continuous CS and SB box girders is significant. Under a uniform load, both the tensile stress on the top slab and compressive stress on the bottom slab increased. For example, the tensile stress at the intersection of the top slab and web increased by 11.3 %, while the compressive stress at the intersection of the bottom slab and web increased by 13.1 %. Under concentrated loads, the self-equilibrium conditions increased or decreased the stress at different positions of the top and bottom slabs. For example, the tensile stress at the intersection of the top slab and web decreased by 19.1 %, which is beneficial for composite box girders. In addition, under both concentrated and uniform loads, the influence of the self-equilibrium conditions was greater at other positions of the flange slabs; however, the stress at other positions was relatively small. Similarly, the actual effect is not prominent. Therefore, if the effect of self-equilibrium conditions is not considered under continuous boundary conditions, the mechanical analysis results in this study will poorly reflect the actual mechanical properties of continuous CS and SB box girders.

5. Conclusion

In this study, factors such as the accordion effect, self-equilibrium conditions for the shear-lag warping stress and bending moment, shear lag, and Timoshenko shear deformation were comprehensively considered, leading to a more reliable theoretical basis for CS and SB box girders. The proposed model reflects the internal mechanisms of CS and SB box girders and is in good agreement with finite element numerical solutions and experimental results. In particular, compared with the traditional theory, the algorithm derived in this study demonstrates the importance of introducing self-equilibrium conditions for continuous CS and SB box girders.

The SB slab was the main object of influence of the accordion effect and self-equilibrium condition. For simply supported box girders, the influence of these conditions was greater under concentrated loads. For the continuous boundary conditions, the effect was more prominent under a uniform load. In particular, the experimental model beam was an actual small-span bridge based on the similarity theory, and the normal stress on the SB slab of the model beam was more than 20 times that of the RC top slab. However, according to the Chinese Bridge Design Specification, the design strength ratio of the SB slab and RC top slab material is 13.6. Therefore, designers should rely on measures to avoid problems, such as yielding and buckling of the SB slab and cracking of the RC top slab.

The CS and SB box girders have some mechanical defects, such as a higher neutral axis and an unreasonable stress distribution on the steel bottom slab and RC top slab. However, refined mechanical analyses can help correct these mechanical defects during the design stage; for example, a reasonable layout of the prestressed reinforcement. At the same time, because the accordion effect weakened the mutual restraint between the flange slabs and webs, the dead weight of this type of structure is substantially reduced. In particular, CS and SB box girders are more suitable for bridge construction in areas with large temperature differences, collapsible loess, and soft soil. Therefore, composite box girders with CS webs and SB slabs is worth recommending and applying in bridge engineering.

Acknowledgement

The authors would like to gratefully acknowledge the financial support from the National Natural Science Foundation of China (Grant No. 51908285).

REFERENCES

[1] Hugo, C., Gomez, P.J., Fanning, M.Q., Feng, S.L.: Testing and long-term monitoring of a curved concrete box girder bridge, Engineering Structures, 33 (2011) 10, pp. 2861-2869, https://doi.org/10.1016/j.engstruct.2011.05.026

[2] Jin, Y., Sun, C., Liu, H., Xu, D.: Analysis on the causes of cracking and excessive deflection of long span box girder bridges based on space frame lattice models, Structures, 2023, 50: pp. 464-481, https://doi.org/10.1016/j.istruc.2022.11.014.

[3] Guiglia, M., Taliano, M.: Experimental analysis of the effective prestress in large-span bridge box girders after 40 years of service life, Engineering Structures, 66 (2014), pp. 146-158, http://doi.org/10.1016/j.engstruct.2014.01.021.

[4] Li, L., Zhou, C., Wang, L.: Distortion analysis of non-prismatic composite box girders with corrugated steel webs, Journal of Constructional Steel Research, 147 (2018), pp. 74-86, https://doi.org/10.1016/j.jcsr.2018.03.030.

[5] Nie, J.G., Zhu, Y.J., Tao, M.X., Guo, C.R.:. Optimized prestressed continuous composite girder bridges with corrugated steel webs, Journal of Bridge Engineering, 22 (2017) 2, pp. 1-17, https://doi.org/10.1061/(ASCE)BE.1943-5592.0000995.

[6] Zhu, Y., Shen, K., Wan, S., Brigham, J.C., Fascetti, A., Zhou, P.: Torsional repair of damaged single-box multi-cell composite box-girder with corrugated steel webs using CFRP. Part I: Experimental investigation, Composite Structures, 296 (2022), Paper 115920, https://doi.org/10.1016/j.compstruct.2022.115920.

[7] Oh, J.Y., Lee, D.H., Kim, K.S.: Accordion effect of prestressed steel beams with corrugated webs, Thin-Walled Structures, 57 (2012),pp. 49-61, http://dx.doi.org/10.1016/j.tws.2012.04.005.

[8] Sui-di, S., Ke-jian, C., Ming, Y.: Study of ultimate spans of continuous rigid-frame bridges with corrugated steel webs, Bridge Construction, 47 (2017) 4, pp. 72-77

[9] He, J., Liu, Y., Wang, S., Xin, H., Chen, H., Ma, C.: Experimental study on structural performance of prefabricated composite box girder with corrugated webs and steel tube slab, Journal Of Bridge Engineering, 24 (2019) 6; Paper 04019047, https://doi.org/10.1061/(ASCE)BE.1943-5592.0001405.

[10] Kumar, S.A., Sofi, F.A., Bhat, J.A.: Equivalent flat-web thicknesses and modified flange-based moment resistance for corrugated-web steel I-girders, Journal of Constructional Steel Research, 207 (2023), Paper 107946, https://doi.org/10.1016/j.jcsr.2023.107946.

[11] Gong, B., Liu, S., Mao, Y., Qin, A., Cai, M.: Correction of shear lag warping function of steel bottom - Corrugated steel web box girder, Structures, 37 (2022), pp. 227-241, https://doi.org/10.1016/j.istruc.2021.12.084.

[12] Zichen, Z., Wang, G., Jiang, F., Xuejun, J.: Natural vibration characteristics of continuous box composite girder with corrugated steel webs of uniform cross-section, China Railway Science, 42 (2021) 4, pp. 51-59. (in Chinese)

[13] Jiang, R.J., Kwong Au, F.T., Xiao, Y.F.: Prestressed concrete girder bridges with corrugated steel webs: review, Journal of Structural Engineering, 141 (2014) 2, Paper 04014108, https://doi.org/10.1061/(ASCE)ST.1943-541X.0001040.

[14] Jiang, R., Wu, Q., Xiao, Y., Peng, M., Au, T.K., Xu, T., Chen, X.: The shear lag effect of composite box girder bridges with corrugated steel webs, Structures, 48 (2023), pp. 1746-1760, https://doi.org/10.1016/j.istruc.2023.01.031.

[15] Deng, W., Liu, D., Peng, Z., Zhang, J.: Behavior of cantilever composite girder bridges with CSWs under eccentric loading, KSCE Journal of Civil Engineering, 25 (2021) 10, pp. 3925-3939, https://doi.org/10.1007/s12205-021-2328-3

[16] Lertsima, C., Chaisomphob, T., Yamaguchi, E., Sa-nguanmanasak, J.: Deflection of simply supported box girder including effect of shear lag, Computers & Structures, 84 (2005) ½, pp. 11-18, https://doi:10.1016/j.compstruc.2005.

[17] Ye, M., Li, L., Yoo, D.Y., Wang, L., Li, H., Zhou, C.: Shear performance of prestressed composite box beams with ultra-high-performance concrete and corrugated steel webs under different loading conditions, Thin-Walled Structures, 186 (2023), Paper 110675, https://doi.org/10.1016/j.tws.2023.110675.

[18] Zhou, M., Chen, Y., Su, X., An, L.: Mechanical performance of a beam with corrugated steel webs inspired by the forewing of Allomyrina dichotoma, Structures, 29 (2021), pp. 741-750, https://doi.org/10.1016/j.istruc.2020.12.001

[19] Kövesdi, B., Dunai, L.: Fatigue life of girders with trapezoidally corrugated webs: An experimental study, International Journal of Fatigue, 64 (2014), pp. 22-32, http://dx.doi.org/10.1016/j.ijfatigue.2014.02.017.

[20] Sherif, A.I., Wael, W., El-Dakhakhni, M.E.: Behavior of bridge girders with corrugated webs under monotonic and cyclic loading, Engineering Structures, 28 (2006) 14, pp. 1941-1955.

[21] Aggarwal, K., Wu, S., Papangelis; j.: Finite element analysis of local shear buckling in corrugated web beams, Engineering Structures, 162 (2018), pp. 37-50, https://doi.org/10.1016/j.engstruct.2018.01.016.

[22] Wei, W.: Ansys 14.0 Finite Element Analysis for Civil Engineering [M]. Beijing: Tsinghua University Press, 2013.